https://dx.doi.org/10.1016/j.ces.2022.117816

New nitrogen-doped graphitic carbon nanosheets with rich structural defects and hierarchical nanopores as efficient metal-free electrocatalysts for oxygen reduction reaction in Zn-Air batteries

Jie Yu[a, +], Yawen Dai [a, +], Zhenbao Zhang [a], Tong Liu [a], Siyuan Zhao [a], Qijiao He [a], Peng Tan [b], Zongping Shao [c, d, *], Meng Ni [a, *]

[a] *Department of Building and Real Estate, Research Institute for Sustainable Urban Development (RISUD) and Research Institute for Smart Energy (RISE), The Hong Kong Polytechnic University, Hung Hom, Kowloon, Hong Kong 999077, China*
[b] *Department of Thermal Science and Energy Engineering, University of Science and Technology of China, Hefei 230026, Anhui, P. R. China*
[c] *State Key Laboratory of Materials-Oriented Chemical Engineering, College of Chemical Engineering, Nanjing Tech University, No. 30 PuZhu South Road, Nanjing, 211800, P. R. China*
[d] *Department of Chemical Engineering, Curtin University, Perth, Western Australia 6845, Australia*
[+] Jie Yu and Yawen Dai equally contributed to this work.

[*]Corresponding author:
Tel: +86-25-83172256 (Z. P. Shao); +852-27664152 (M. Ni)
E-mail address: shaozp@njtech.edu.cn (Z. P. Shao); meng.ni@polyu.edu.hk (M. Ni)

ABSTRACT

Carbon materials are highly promising alternative metal-free catalysts for oxygen reduction reaction (ORR), an important element reaction involved in various energy storage/conversion processes, while controllable and fine structural and morphological tunning is key for maximizing the catalytic performance. Here, we report the rational design of hierarchical porous graphitic carbon nanosheets with rich defects (d-pGCS) based on a facile two-step thermal treatment route, delivering superior catalytic ORR performance in alkaline electrolytes. The second thermal treatment is critical in creating such structural defects and nanopores. Through optimizing synthesis parameters, d-

pGCS-1000 exhibits outstanding electrocatalytic ORR performance in terms of positive onset potential (0.95V), half-wave potential (0.82V), and limiting current density (6.02 mA cm^{-2}). As a proof-of-concept, the obtained Zn-air battery delivers a large open-circuit voltage (1.42V), high peak power density (182.8 mW cm^{-2}), high specific capacity (773 mAhgZn^{-1}), and good rate performance. Such results are comparable to or even better than the Pt/C-based Zn-air battery.

Keywords: Carbon nanosheets; structural defects; hierarchically porous structure; oxygen reduction reaction; Zn-air battery

1. Introduction

Oxygen reduction reaction (ORR) involves in many electrochemical energy conversion and storage processes, such as Zn-air batteries (ZABs) and fuel cells, and its behavior could largely affect the economical competitiveness and widespread application capability of these new technologies. Due to their large theoretical energy density, environmental harmlessness, and high operation safety, ZABs have been recognized as highly promising next-generation energy conversion devices, which can be used as the power source for electrical vehicles or even large-scale energy storage (Dai et al., 2020a; Lu et al., 2019; Sun et al., 2021; Wang et al., 2022). Unfortunately, owing to the high activation energy associated with the oxygen reduction process, the ORR usually shows sluggish reaction kinetics at room temperature, which severely impairs the overall efficiency and performance of conventional ZABs, and unavoidably becomes a big bottleneck in their practical applications (Dhavale and Kurungot, 2015; Zhang et al., 2021.). To accelerate the ORR kinetics, some appropriate electrocatalyst is needed. Up to now, the state-of-art ORR electrocatalysts still lean upon Pt-based materials (Amiinu et al., 2018; Lv et al., 2020; Wu et al., 2021; Yu et al., 2020a), while the scarcity, costliness, and poor stability of Pt inhibit their large scale use. Instead,

alternative ORR electrocatalysts with high efficiency, low cost, and robust long-term durability are urgently demanded (Cai et al., 2017; Ren et al., 2020; Wu et al., 2020a; Yu et al., 2017).

From the cost consideration, considerable research efforts have been devoted to the development of non-noble metal-based oxygen-reduction electrocatalysts, including transition-metal oxides, transition-metal carbides, transition-metal nitrides, transition-metal chalcogenides, metal-free carbon, metal-carbon composite, etc (Dai et al., 2020b; Lv et al., 2018; Wang et al., 2018b; Wang et al., 2021; Yan et al., 2017; Yu et al., 2016b; Yu et al., 2020b). Notedly, functional metal-free carbon materials, because of their low cost, high abundance, large conductivity, and robust durability under severe conditions, have aroused substantial attention in the ORR electrocatalysis (Yu et al., 2016a; Zhang et al., 2015). Heteroatom doping (N, P, S, B, etc.) has been extensively tried to modify the electronic structure of carbonaceous materials, to induce superior catalytic activity for ORR, which could be even comparable to Pt-based catalysts (Jiang et al., 2019; Mulyadi et al., 2017; Yang et al., 2011; Zhang et al., 2020a). The origin of such favorable activity is from the modulation and redistribution of the charge density of adjacent carbon atoms by the doped heteroatoms, leading to the easy adsorption of molecular oxygen and the creation of more ORR active sites (Yang et al., 2020). For example, Wu and his co-workers reported nitrogen-doped vertical graphene (NVG) nanosheets as highly active metal-free electrocatalyst toward ORR, which was prepared by a novel N_2 plasma-enhanced chemical vapor deposition (PECVD) method (Wu et al., 2020b). Benefiting from the high nitrogen doping content and a controllable vertical nanostructure, when operating under alkaline conditions, the optimal NVG-30 sample delivered the best ORR performance and the half-wave potential was 0.80 V vs. RHE. Recently, our team also constructed carbon-based materials with rich N dopants which

displayed impressive ORR catalytic activity (Yu et al., 2016a; Yu et al., 2017).

In addition to doping, recently, defect engineering was also exploited for enhancing ORR activity (Jia et al., 2016; Jiang et al., 2015; Tang and Zhang, 2017; Yan et al., 2016; Zhao et al., 2015). By means of experimental and theoretical tools, Hu's group found pentagon and zigzag edge carbon defects in their obtained defective carbon nanocages were responsible for the outstanding ORR performance (Jiang et al., 2015). Yao's team also proposed that structural carbon defects (e.g., 5-8-5 defects, edge pentagon defects, etc.) were more effective than heteroatom doping in enhancing ORR catalytic activity (Jia et al., 2016; Yan et al., 2016; Zhao et al., 2015). Therefore, defect engineering is also highly attractive for the development of efficient carbon-based catalysts for ORR. In addition to structural features (alien dopant and defects), the morphology also plays an important role in determining the apparent activity of the electrocatalysts since it may affect the number of active sites and mass transfer resistance (Pampel and Fellinger, 2016; Wang et al., 2018a). To address the problem, rational design and construction of a hierarchically macro/mesoporous nanostructure and large specific area in the catalytic material are extremely beneficial to accelerate rapid mass exchanges and enhance the transfer kinetics.

Simultaneous doping, defect engineering, and morphology control could then maximize the reaction sites and intrinsic activity, thus bringing the optimal catalytic activity of carbon materials for ORR. Herein, we reported a simple two-step heat treatment strategy to fabricate novel nitrogen-doped graphitic carbon nanosheets with rich structural defects and hierarchical pores (d-pGCS) as superior ORR electrocatalysts, demonstrating outstanding performance. Through optimization, the derived nitrogen-doped carbon catalyst (d-pGCS-1000) demonstrated outstanding catalytic activity even comparable to the benchmark Pt/C while offering much more

robust operational durability, particularly under methanol conditions, in alkaline solution. The experimental characterizations confirmed that the obtained carbon material possessed abundant topological defects and a plentiful hierarchically porous nanostructure. Finally, the constructed primary Zn-air batteries with d-pGCS-1000 as cathode displayed excellent discharge performance, including the high peak power density, large specific capacity, and good rate, demonstrating the practical application of this d-pGCS-1000 electrocatalyst.

2. Results and discussion

2.1. Synthesis and structural characterization

The synthesis process of d-pGCS was given in Fig. 1, which diagrammatically described the pyrolysis products in different stages. Here, ethylenediaminetetraacetic acid (EDTA), glucose, and melamine were used as the main raw materials, which performed as the carbon and nitrogen sources After the first pyrogenic decomposition at 800 ºC, an N-rich carbon framework, named NrC, was obtained. Subsequently, a second heating treatment at a higher temperature (900-1100 ºC) was conducted in an inert atmosphere to induce the formation of a graphene-like structure with high graphitization and rich topological defects, which was called as d-pGCS-T (T = 900, 1000, or 1100). The structural features and morphology of both NrC and d-pGCS were characterized by various techniques and they were also applied as model electrocatalysts for ORR.

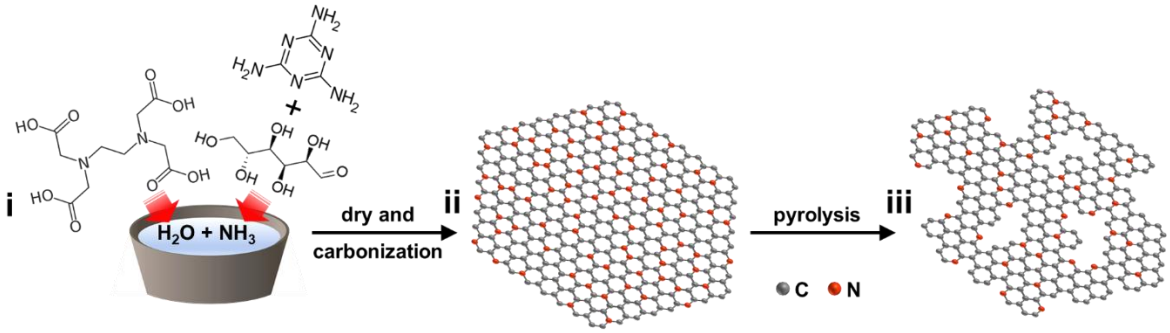

Fig. 1. Schematic description of the fabricated procedure of d-pGCS-T.

The phase structure of the synthesized samples (NrC and d-PGCS) was first characterized by room-temperature powder X-ray diffraction (XRD) with the typical patterns shown in Fig. S1. Two broad diffraction peaks centered at 2-theta of 23~25 º and 40~45º were observed for both samples, which are characteristic peaks of carbon materials, suggesting the successful formation of graphic carbon even after the first-step calcination. Noticeably, the d-pGCS sample from a further thermal treatment of NrC at higher temperature showed the stronger and more obvious characteristic peaks, which slightly shifted to the higher angles as compared to that of NrC. These results indicate that a second thermal treatment at a higher temperature enhanced the degree of graphitization, which is beneficial for enhancing the electrical conductivity of the samples.

The morphology of the synthesized carbon materials was first observed by Scanning electron microscopy (SEM) with the typical images shown in Fig. S2. The as-prepared NrC sample from one-step calcination presented a typical interconnected three-dimensional (3D) morphological structure which was built by layered nanosheets. After being conducted a further thermal treatment at 900-1100 ºC, the derived d-pGCS materials exhibited an analogous macroscopic morphology to NrC, but with more surface-wrinkling, and thinner graphene-like nanolayers, as shown in Fig. 2(a) and S2. To get more detailed information on the microstructure, the d-pGCS-1000 sample was selected for further observation by transmission electron microscopy (TEM). As shown in Fig. 2(b) and S3, a clear wrinkle-abundant and thin laminated structure was demonstrated at the nanoscale range. According to the high-resolution TEM image of the d-pGCS-1000, the graphene-like nanosheets have few-layer features with rich nanosized holes in the plane (Fig. 2(c)). Besides, some lattice defects were found from

a closer observation (Fig. 2(d)). These defects might be originated from the thermal treatment, which was believed to alter the catalytic properties of carbon materials (Jia et al., 2016; Yan et al., 2016; Zhao et al., 2015). Furthermore, the homogeneous distribution of N, C, and O on the carbon scaffold of d-pGCS-1000 was demonstrated by the elemental mappings in Fig. 2(e), which suggested its nitrogen-doped nature. The oxygen is likely due to the adsorption from the air condition. Both EDTA and melamine likely performed as the nitrogen sources while glucose mainly acted as the carbon source. The synergy played among the three samples in the precursor during the pyrolysis led to the formation of the nitrogen-doped carbon material with a specific morphological structure.

The nanostructure ensures a high surface area for proving rich active sites while the porous structure allows the free mass transfer, which thus benefits the ORR. The specific surface areas and porosities of the as-prepared samples were then assessed by nitrogen adsorption/desorption with the corresponding adsorption-desorption isotherms with the typical IV type shown in Fig. 2(f) and S4, which indicated the presence of the mesoporous structure for all samples (Su et al., 2021). The NrC from one-step calcination possessed a specific surface area of 292.3 m^2 g^{-1} and a total pore volume of 2.23 cm^3 g^{-1}. In addition, there is an obvious main peak at below 2 nm in the pore-size distribution curve, revealing the presence of abundant micropores. After the further thermal treatment at 900 ºC, the derived d-pGCS-900 sample showed an increase in specific surface area to 394.1 m^2 g^{-1}. Interestingly the total pore volume kept almost no change (2.23 cm^3 g^{-1}), while the pore-size distribution altered significantly with negligible micropores. With the increase in the thermal treatment temperature at the second calcination step, the specific surface area and the total pore volume were gradually decreased, while the pore-size distribution curves were very similar for all

the d-pGCS samples. For the d-pGCS-1000 sample, the specific surface area and total pore volume were 301.6 m^2 g^{-1} and 1.56 cm^3 g^{-1}, respectively, and a large number of mesopores around 4 nm appeared. Combining with the evidence of macropore structure from the microscopy observation, it suggests the hierarchically porous nature of all the d-pGCS samples. Based on previous reports, the macropores and mesopores in electrocatalysts can facilitate the transport of ORR-related species, thus benefiting the ORR efficiency (Liang et al., 2014; Xiao et al., 2015).

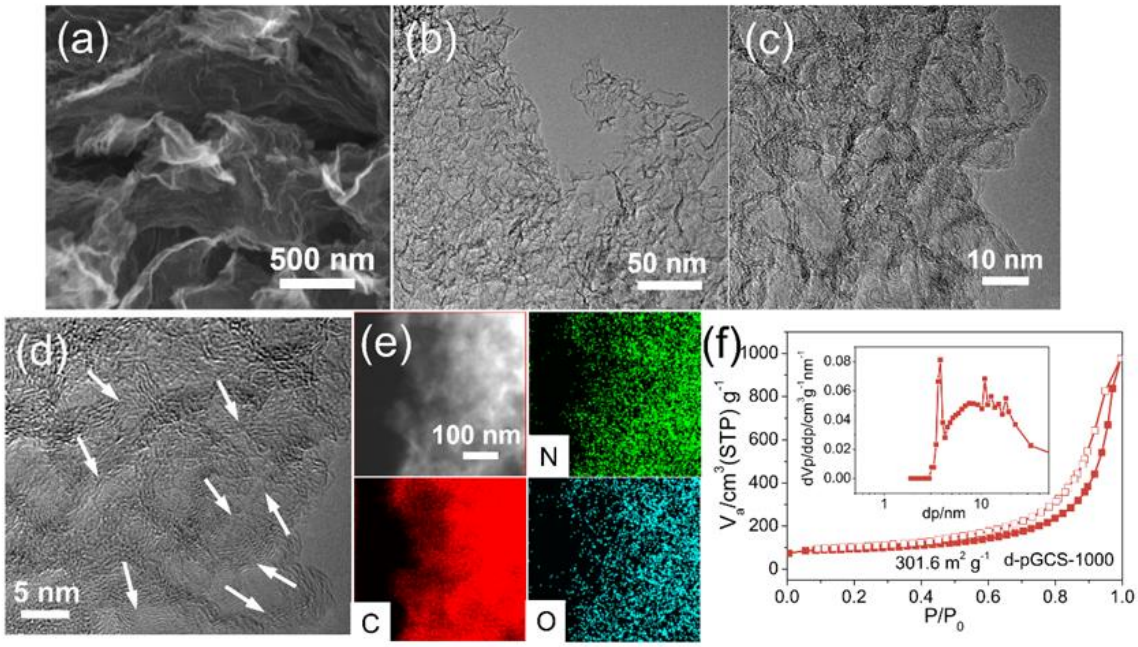

Fig. 2. (a) SEM, (b) TEM, and (c, d) HR-TEM images of d-pGCS-1000. (e) EDX elemental distribution images of d-pGCS-1000. (f) N_2 adsorption/desorption isotherm and the corresponding pore-size distribution images of d-pGCS-1000.

2.2. Electrochemical measurements

The electrocatalytic activities of all the as-prepared d-pGCS samples, NrC, and commercial Pt/C toward ORR were comparatively studied in the 0.1 M KOH electrolyte. Fig. 3(a) compared the cyclic voltammetry (CV) curves within the potential region from 0.15 to 1.05 V in N_2- or O_2-saturated solution. Remarkably, both d-pGCS-1000 and NrC catalysts showed the flat CV curves under N_2-saturated conditions

because of lacking the faradaic process, whereas well-defined redox peaks were found for both of them in O_2-saturated electrolyte, which revealed that the electrocatalytic activity originated from the oxygen reduction process. Moreover, the peak potential of d-pGCS-1000 is 0.79 V, substantially larger than 0.73 V of NrC, confirming the better ORR activity of d-pGCS-1000 than NrC. Linear scan voltammogram (LSV) curves of all samples at a rotation speed of 1600 rpm were obtained to further assess the ORR activity. As exhibited in Fig. 3(b), all d-pGCS samples possessed obviously better ORR activities than that of NrC, especially in the aspects of onset potential (E_{onset}) and half-wave potential ($E_{half\text{-}wave}$) (Fig. 3(c)). This suggested a second thermal treatment at a higher temperature played an important role in enhancing the ORR activity of the catalysts, and the origin of such improvement will be discussed further later. Among all the tested d-pGCS catalysts, d-pGCS-1000 showed the most outstanding ORR activity with the onset potential of 0.95 V, half-wave potential of 0.82 V, and the limiting current density of 6.02 mA cm^{-2}. By comparing to the commercial Pt/C, the E_{onset} and $E_{half\text{-}wave}$ values of d-pGCS-1000 were found to be slightly worse (0.99 and 0.85 V), while the limiting current density of d-pGCS-1000 is much larger (5.39 mA cm^{-2}). Accordingly to a comparison of the performance for some typical metal-free catalysts, as reported in literature very recently, the performance of the developed d-pGCS-1000 catalyst in this study ranked ahead of them (Table S1). It thus highly promises d-PGCS-1000 as a metal-free ORR electrocatalyst for operating in alkaline media.

To reflect the kinetic properties, the Tafel plots, derived from LSV curves, were also studied and given in Fig. 3(d)**.** Typically, a smaller Tafel slope means a superior ORR activity with better reaction kinetics. The d-pGCS-1000 catalyst showed a Tafel slope of 96 mV dec^{-1}, which was the lowest one among d-pGCS and NrC samples and was comparable to that of the Pt/C benchmark (71 mV dec^{-1}). LSV testing at various

rotating speeds (400, 800, 1200, 1600, 2000, and 2500 rpm) was further carried out for in-depth understanding of the reaction mechanism, and Fig. 3(e), (f), and S5 presented the corresponding LSV curves of d-pGCS-1000, NrC, and Pt/C, respectively. With the increase of the rotation rates, the limiting current densities became larger, but the E_{onset} values kept constant. On basis of these LSV curves, the Koutecky-Levich (K-L) plots of d-pGCS-1000, NrC, and Pt/C were prepared. The well linear feature of these plots demonstrated the first-order kinetics toward the concentration of dissolved oxygen. The transferred electron number for this d-pGCS-1000 catalyst was determined to be 3.8, which was analogous to the value of Pt/C (4.0), indicative of a quasi four-electron-transfer ORR pathway. This result provided additional solid evidence of the remarkable ORR activity of d-pGCS-1000.

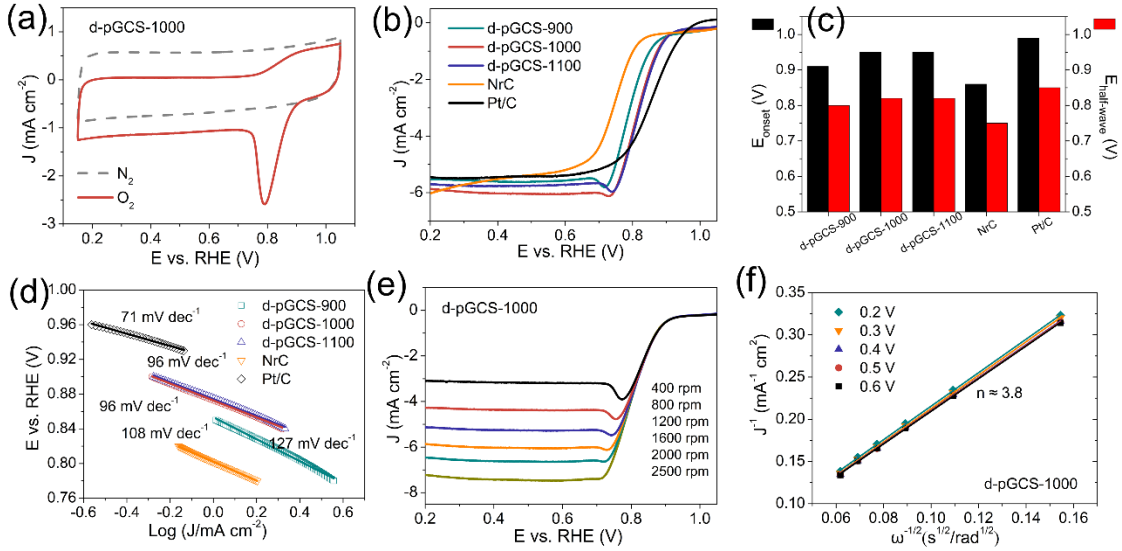

Fig. 3. (a) CV curves in O_2 and N_2-saturated KOH electrolytes for this d-pGCS-1000 sample. (b) The ORR polarization curves of NrC, all d-pGCS-T catalysts, and Pt/C under 0.1 M KOH condition. (c) The comparison of onset potentials (E_{onset}) and half-wave potentials ($E_{half\text{-}wave}$) of all catalytic samples. (d) The ORR Tafel plots of NrC, d-pGCS-T, and Pt/C catalysts. (e) The polarization curves at different rotation speeds (400-2500 rpm) and (f) the corresponding K-L plots of d-pGCS-1000.

In addition to the excellent ORR activity, all d-pGCS samples also demonstrated favorable durability as disclosed by the chronoamperometric response at the fixed voltage of 0.6 V (Fig. 4(a) and S6). d-pGCS-1000 still preserved 98% of the initial current even after the continuous test for a period of 12 h, slightly higher than those values of d-pGCS-900 (93%) and d-pGCS-1100 (95%). In contrast, the ORR current declined to 82 % of the initial value for commercial Pt/C following the same 12 h test duration. Such a reduction in the performance of the Pt/C catalyst could be caused by aggregation and escapement of Pt nanoparticles supported on carbon substrate during the long-period operation (Xu et al., 2020). By comparing the LSV curves obtained before and after 1000 cycles based on the accelerated durability testing (ADT), the d-pGCS-1000 electrocatalyst exhibited no evident change in the onset and half-wave potentials (Fig. 4(b)), which further indicated the superior stability of d-pGCS-1000. Furthermore, the catalytic sensitivity against methanol for d-pGCS-1000 and Pt/C was also studied by adding methanol into the aqueous alkaline electrolyte in the chronoamperometric measurement (i-t) (Fig. 4(c)). The response current of the d-pGCS-1000 catalyst had no conspicuous change in presence of methanol, validating the strong methanol tolerance of the d-pGCS-1000 catalyst. Conversely, a sharp drop in the current density was observed for the Pt/C catalyst over the i-t testing course after the addition of methanol, indicating a rapid ORR-activity degradation owing to methanol poisoning.

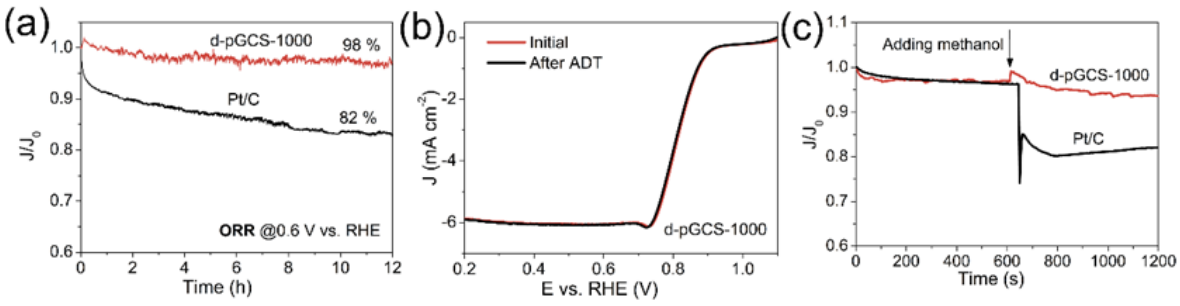

Fig. 4. (a) The chronoamperometric response at the fixed voltage of 0.6 V for d-pGCS-1000 and Pt/C samples. (b) The ADT curves before and after 1000 cycles for d-pGCS-1000. (c) The i-t curves of d-pGCS-1000 and Pt/C samples at 0.6 V in 0.1 M KOH before and after the addition of methanol.

2.3. The origins for the enhanced performance of d-pGCS-1000

Exploiting the origin of the outstanding ORR performance for the d-pGCS-1000 catalyst will help to offer useful guidance for future development and design of excellent metal-free carbon catalytic materials. As generally known, conventional pure carbon-based electrocatalysts delivered relatively poor ORR behavior with a two-electron ORR pathway (Su et al., 2021; Yang et al., 2019). Nevertheless, it is widely accepted that the incorporation of heteroatoms, especially N, into the carbon lattice can alter the electronic structure of carbon and thus strengthen oxygen chemisorption and reduction, favoring the ORR process (Guo et al., 2016; Wei et al., 2021). According to the XPS analysis results (Table S2), the initial NrC had a high N content, i.e. ~12.22 at%, while the further heat treatment induced the reduction of N concentration and the N content of the most outstanding d-pGCS-1000 material was ~3.37 at %. Such findings revealed that nitrogen doping is not the sole cause for the high ORR performance of d-pGCS-1000. The O atomic concentration in all samples was also further analyzed by XPS results. Obviously, the O content in all three d-pGCS samples is larger than that of NrC, and the d-pGCS-1000 sample displayed the highest O content, which suggested a higher O_2 adsorption ability on d-pGCS-1000 (Table S2 and Fig. 5(a)). Considering the adsorption of O_2 on the surface of a catalyst is a crucial step in the ORR process, a stronger O_2 adsorption is favorable to ORR (Su et al., 2021). Fig. 5(b) and S7 presented the high-resolution C 1s spectra, which could be deconvoluted into five subpeaks, assigned to C-C (≈285.0 eV), C-O&C=N (≈285.7 eV), C=O&C-N (≈286.6 eV), and

O=C-O (≈289.5 eV), respectively (Hao et al., 2021). It further disclosed that d-pGCS-1000 possessed richer oxygen functional groups, which could bring about extra chemical binding interactions with reactants in the ORR process. A large amount of carbon-oxygen functional groups on the surface of d-pGCS-1000 possibly indicated the presence of abundant defects over the carbon (Su et al., 2021). These exposed defects are electron-deficient and thus are prone to interact with water or oxygen in the electrolyte.

Raman spectra of the various samples were also characterized with the results shown in Fig. 5(c). Two distinct peaks at ~1580 cm^{-1} (G band) and 1350 cm^{-1} (D band) were observed, corresponding to the graphitic carbon structure and the defect on the disordered carbon, respectively (Yu et al., 2016a). Clearly, the NrC had a high peak intensity ratio of D/G band (I_D/I_G), i.e., 1.01, which reflected the large defect degree. Here, the defect should stem from the introduction of plentiful N atoms into the carbon framework. As comparison, the I_D/I_G values of these d-pGCS samples were slightly lowered. They are 0.94, 0.95, and 0.95 for d-pGCS-900, d-pGCS-1000, and d-pGCS-1100, respectively. Indeed, a higher-temperature treatment in carbon materials could boost the larger graphitization, that is in favor of the enhanced conductivity, which was further confirmed by the lower charge transfer resistance (R_{ct}) from the electrochemical impedance spectroscopy (EIS) measurements (Fig. S8). However, plenty of defect structures still existed in these samples. As stated previously, further heating treatment would remove the doped N atoms, which was in agreement with the XPS results, and many topological defects were generated during the N-removal process. (Wang et al., 2018a) It has been demonstrated that topological defects in carbon materials showed high activity toward the ORR process owing to unsaturation in the electronic structures of the carbon atoms, which was even more effective for ORR than N doping under

certain conditions (Yan et al., 2016; Zhao et al., 2015). Thus, here, the topological defects could become the main contributor to the ameliorated ORR behavior.

As demonstrated above, d-pGCS-1000 possessed a large specific surface area and abundant hierarchically porous structure, which facilitates the contact between reactants and provides more active sites, respectively. Besides, the hierarchically porous structure could enhance the penetration of the liquid electrolyte solution, leading to the vastly boosted charge transfer. Consequently, an enhancement in ORR catalytic activity is expected for the d-pGCS-1000 catalyst as compared to the NrC catalyst. Based on the above analysis, a possible ORR mechanism over the NrC and d-pGCS-1000 catalysts under alkaline conditions was proposed and diagrammatically described in Fig. 5(d).

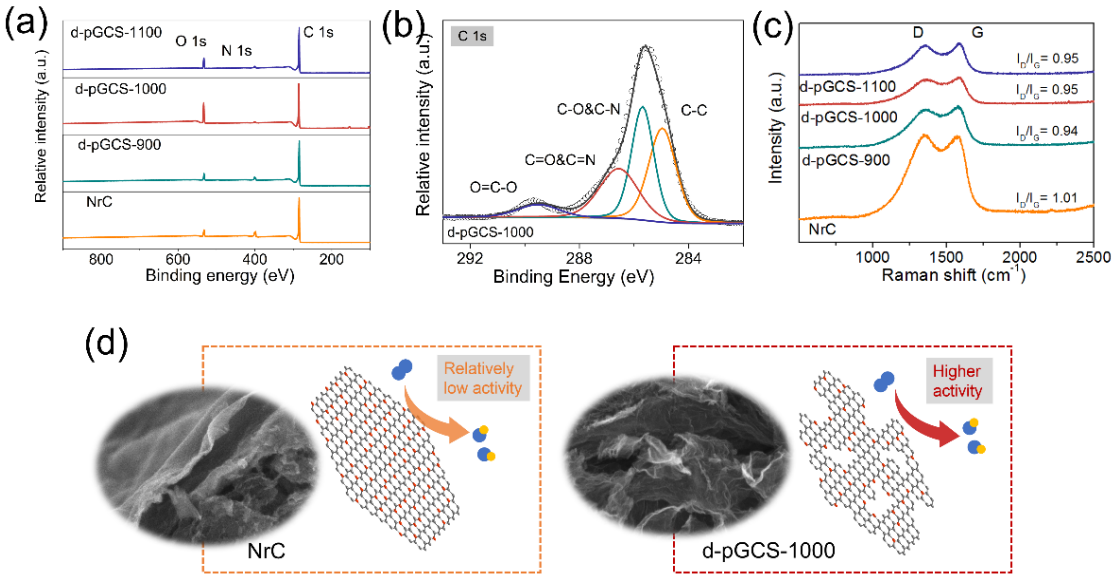

Fig. 5. (a) The full survey spectra of NrC and d-pGCS-T. (b) The high-resolution C 1s XPS spectrum of d-pGCS-1000. (c) Raman spectra of NrC and d-pGCS-T. (d) The proposed ORR mechanism over the NrC and d-pGCS-1000 catalysts.

2.4. Zn-air battery performance

The potential application of d-pGCS-1000 material in practical devices was then exploited by building a primary Zn-air battery (pZAB) with it supported on carbon

paper as the air electrode, Zn plate as the anode, and 6 M KOH + 0.2 M $Zn(Ac)_2$ as the electrolyte (Fig. 6(a)). Clearly, the pZAB provided a high open-circuit voltage (OCV) of 1.42 V (Fig. 6(b)), which was very close to the value of Pt/C-based pZAB (1.45 V). Fig. 6(c) displayed the discharging polarization curves and corresponding power densities plots. Initially, in the low current density (< about 200 mA cm^{-2}), the discharge voltage of the pZAB with the d-pGCS-1000 air electrode was lower than that of the cell with the Pt/C cathode, but it surpassed that of Pt/C when the discharge current density increased to larger than 200 mA cm^{-2}. Such a result suggests that d-pGCS-1000 possessed a better fast discharging performance than the Pt/C benchmark. The peak power density of the pZAB reached as high as 182.8 mW cm^{-2}, exceeding that of the Pt/C-based pZAB (176.6 mW cm^{-2}) and also comparable to many recently developed metal-free carbon materials (**Table S3**). The good mass transport derived from large surface area and porous structure and rich exposed defect sites could account for the excellent discharge performance, especially when O_2 consumption was fast at the high discharging current densities. The rate performance of the pZABs with d-pGCS-1000 and Pt/C air electrodes at various current densities was shown in Fig. 6(d) and (e). With the increase of the discharge current, the discharge potential declined for both pZABs. Notably, when the current density was restored to the original values, the discharge potential of the d-pGCS-1000-based pZAB was well recovered with almost no attenuation, but the Pt/C-based pZAB delivered slightly lower discharge voltages. Such findings demonstrated that the pZAB with the d-pGCS-1000 air electrode had a better rate performance and more outstanding reversibility than the cell with the Pt/C air electrode. As illustrated in Fig. 6(f), the calculated specific capacity of the d-pGCS-1000-based pZAB at 5 mA cm^{-2} is 773 mAh g_{Zn}^{-1}, which is obviously higher than that in the Pt/C-based pZAB (650 mAh g_{Zn}^{-1}). These observations highly promise d-pGCS-

1000 as a metal-free carbon electrocatalyst in practical electrochemical devices.

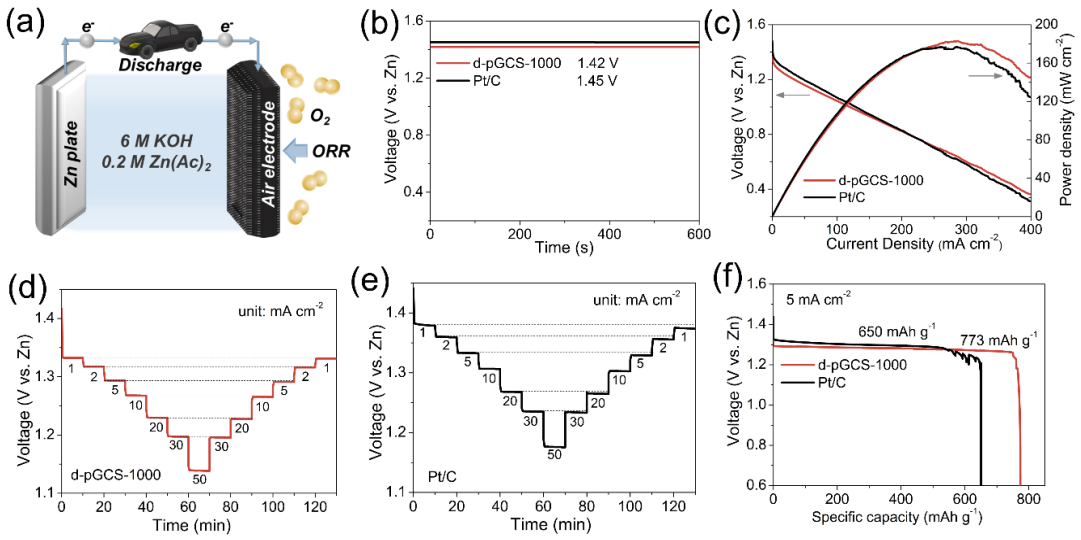

Fig. 6. (a) Schematic illustration of the primary ZAB. (b) The OCV plots of the as-assembled d-pGCS-1000-based and Pt/C-based pZABs. (c) The polarization and power density curves of the fabricated pZABs with d-pGCS-1000 or Pt/C. (d, e) The discharge rate performance at different current densities (1, 2, 5, 10, 20, 30, 50 mA cm^{-2}) of the (d) d-pGCS-1000-based pZAB (d) and (e) Pt/C-based pZAB. (f) specific capacity plots at 5 mA cm^{-2} for d-pGCS-1000 and Pt/C.

4. Conclusions

In summary, a novel metal-free nanosheet-shaped carbon material, d-pGCS, with plentiful structure defects and a hierarchical porous framework was rationally designed and synthesized by a facile two-step pyrolysis route. The as-obtained d-pGCS samples were employed as the ORR electrocatalysts under alkaline conditions, among which, the optimized d-pGCS-1000, which was prepared by a second thermal treatment in an inert atmosphere at 1000 ^{o}C, showed the most superior catalytic activity ($E_{half\text{-}wave}$ = 0.82 V), high stability, and robust anti-toxicity to the methanol. A large number of topological defects were created in the sample during the second thermal treatment, which likely became the most possible contributor to the superior ORR activity of d-

pGCS catalysts. In addition, the hierarchically porous nanostructure and high specific surface area increased the active sites and facilitated the mass/charge transport, and provided enough high conductivity, which further contributed to the superior catalytic activity. As a proof-of-concept, by applying d-pGCS as the air electrode in the assembled Zn-air battery, a large OCV value (1.42 V), peak power density (182.8 mW cm^{-2}), specific capacity (773 mAh g_{Zn}^{-1}), and good rate performance, demonstrating its high promise for practical application.

Declaration of Competing Interests

The authors declare that they have no known competing financial interests or personal relationships that could have appeared to influence the work reported in this paper

Acknowledgments

This work is supported by a grant from Collaborative Research Fund (CRF) (Project no. C5031-20G) of Research Grant Council, University Grants Committee, HK SAR.

References

Amiinu, I. S., Liu, X., Pu, Z., Li, W., Li, Q., Zhang, J., Tang, H., Zhang, H. Mu, S., 2018. From 3D ZIF nanocrystals to Co-Nx/C nanorod array electrocatalysts for ORR, OER, and Zn-air batteries. Adv. Funct. Mater. 28, 1704638.

Cai, X., Lai, L., Lin, J., Shen, Z., 2017. Recent advances in air electrodes for Zn–air batteries: electrocatalysis and structural design. Mater. Horizons 4, 945-976.

Dai, Y., Yu, J., Cheng, C., Tan, P., Ni, M., 2020a. Mini-review of perovskite oxides as oxygen electrocatalysts for rechargeable zinc–air batteries. Chem. Eng. J. 397, 125516.

Dai, Y., Yu, J., Ni, M., Shao, Z., 2020b. Rational design of spinel oxides as bifunctional oxygen electrocatalysts for rechargeable Zn-air batteries. Chem. Phys. Rev. 1, 011303.

Dhavale, V. M., Kurungot, S., 2015. Cu–Pt nanocage with 3-D electrocatalytic surface as an efficient oxygen reduction electrocatalyst for a primary Zn–air battery. ACS Catal. 5, 1445-1452.

Guo, D., Shibuya, R., Akiba, C., Saji, S., Kondo, T., Nakamura, J., 2016. Active sites of nitrogen-doped carbon materials for oxygen reduction reaction clarified using model catalysts. Science 351, 361-365.

Hao, X., Jiang, Z., Zhang, B., Tian, X., Song, C., Wang, L., Maiyalagan, T., Hao, X., Jiang, Z.J., 2021. N−Doped Carbon Nanotubes Derived from Graphene Oxide with

Embedment of FeCo Nanoparticles as Bifunctional Air Electrode for Rechargeable Liquid and Flexible All−Solid−State Zinc-Air Batteries. Adv. Sci. 8, 2004572.
Jia, Y., Zhang, L., Du, A., Gao, G., Chen, J., Yan, X., Brown, C.L., Yao, X., 2016. Defect graphene as a trifunctional catalyst for electrochemical reactions. Adv. Mater. 28, 9532-9538.
Jiang, H., Gu, J., Zheng, X., Liu, M., Qiu, X., Wang, L., Li, W., Chen, Z., Ji, X., Li, J., 2019. Defect-rich and ultrathin N doped carbon nanosheets as advanced trifunctional metal-free electrocatalysts for the ORR, OER and HER. Energy Environ. Sci. 12, 322-333.
Jiang, Y., Yang, L., Sun, T., Zhao, J., Lyu, Z., Zhuo, O., Wang, X., Wu, Q., Ma, J., Hu, Z., 2015. Significant contribution of intrinsic carbon defects to oxygen reduction activity. ACS Catal. 5, 6707-6712.
Liang, H.-W., Zhuang, X., Brüller, S., Feng, X., Müllen, K., 2014. Hierarchically porous carbons with optimized nitrogen doping as highly active electrocatalysts for oxygen reduction. Nat. Commun. 5, 1-7.
Lu, Q., Yu, J., Zou, X., Liao, K., Tan, P., Zhou, W., Ni, M., Shao, Z., 2019. Self−catalyzed growth of Co, N−codoped CNTs on carbon−encased CoSx surface: a noble−metal−free bifunctional oxygen electrocatalyst for flexible solid Zn–air batteries. Adv. Funct. Mater. 29, 1904481.
Lv, Q., Si, W., He, J., Sun, L., Zhang, C., Wang, N., Yang, Z., Li, X., Wang, X., Deng, W., 2018. Selectively nitrogen-doped carbon materials as superior metal-free catalysts for oxygen reduction. Nat. Commun. 9, 1-11.
Lv, Q., Wang, N., Si, W., Hou, Z., Li, X., Wang, X., Zhao, F., Yang, Z., Zhang, Y., Huang, C., 2020. Pyridinic nitrogen exclusively doped carbon materials as efficient oxygen reduction electrocatalysts for Zn-air batteries. Appl. Catal. B-Environ. 261, 118234.
Mulyadi, A., Zhang, Z., Dutzer, M., Liu, W., Deng, Y., 2017. Facile approach for synthesis of doped carbon electrocatalyst from cellulose nanofibrils toward high-performance metal-free oxygen reduction and hydrogen evolution. Nano Energy 32, 336-346.
Pampel, J., Fellinger, T.P., 2016. Opening of bottleneck pores for the improvement of nitrogen doped carbon electrocatalysts. Adv. Energy Mater. 6, 1502389.
Ren, S., Duan, X., Liang, S., Zhang, M., Zheng, H., 2020. Bifunctional electrocatalysts for Zn–air batteries: recent developments and future perspectives. J. Mater. Chem. A 8, 6144-6182.
Su, C., Liu, Y., Luo, Z., Veder, J.-P., Zhong, Y., Shao, Z., 2021. Defects-rich porous carbon microspheres as green electrocatalysts for efficient and stable oxygen-reduction reaction over a wide range of pH values. Chem. Eng. J. 406, 126883.
Sun, W., Wang, F., Zhang, B., Zhang, M., Küpers, V., Ji, X., Theile, C., Bieker, P., Xu, K., Wang, C., 2021. A rechargeable zinc-air battery based on zinc peroxide chemistry. Science 371, 46-51.
Tang, C., Zhang, Q., 2017. Nanocarbon for oxygen reduction electrocatalysis: dopants, edges, and defects. Adv. Mater. 29, 1604103.
Wang, Q., Ji, Y., Lei, Y., Wang, Y., Wang, Y., Li, Y., Wang, S., 2018a. Pyridinic-N-

dominated doped defective graphene as a superior oxygen electrocatalyst for ultrahigh-energy-density Zn–air batteries. ACS Energy Lett. 3, 1183-1191.
Wang, X., Zhang, X., Fu, G., Tang, Y., 2021. Recent progress of electrospun porous carbon-based nanofibers for oxygen electrocatalysis. Mater. Today Energy 22, 100850.
Wang, Y.-J., Fan, H., Ignaszak, A., Zhang, L., Shao, S., Wilkinson, D.P., Zhang, J., 2018b. Compositing doped-carbon with metals, non-metals, metal oxides, metal nitrides and other materials to form bifunctional electrocatalysts to enhance metal-air battery oxygen reduction and evolution reactions. Chem. Eng. J. 348, 416-437.
Wang, Y., Wu, X., Jiang, X., Wu, X., Tang, Y., Sun, D., Fu, G., 2022. Citrulline-induced mesoporous CoS/CoO heterojunction nanorods triggering high-efficiency oxygen electrocatalysis in solid-state Zn-air batteries. Chem. Eng. J. 434, 134744.
Wei, P., Li, X., He, Z., Sun, X., Liang, Q., Wang, Z., Fang, C., Li, Q., Yang, H., Han, J., 2021. Porous N, B co-doped carbon nanotubes as efficient metal-free electrocatalysts for ORR and Zn-air batteries. Chem. Eng. J. 422, 130134.
Wu, Z., Wu, H., Niu, T., Wang, S., Fu, G., Jin, W., Ma, T., 2020a. Sulfurated metal-organic framework-derived nanocomposites for efficient bifunctional oxygen electrocatalysis and rechargeable Zn-air battery. ACS Sustain. Chem. Eng. 8, 9226-9234.
Wu, Z., Zhang, Y., Li, L., Zhao, Y., Shen, Y., Wang, S., Shao, G., 2020b. Nitrogen-doped vertical graphene nanosheets by high-flux plasma enhanced chemical vapor deposition as efficient oxygen reduction catalysts for Zn-air batteries. J. Mater. Chem. A 8, 23248-23256.
Wu, Z., Zhao, Y., Jin, W., Jia, B., Wang, J., Ma, T., Recent progress of vacancy engineering for electrochemical energy conversion related applications. Adv. Funct. Mater. 31, 2009070.
Xiao, M., Zhu, J., Feng, L., Liu, C., Xing, W., 2015. Meso/macroporous nitrogen‐doped carbon architectures with iron carbide encapsulated in graphitic layers as an efficient and robust catalyst for the oxygen reduction reaction in both acidic and alkaline solutions. Adv. Mater. 27, 2521-2527.
Xu, Y., Deng, P., Chen, G., Chen, J., Yan, Y., Qi, K., Liu, H., Xia, B.Y., 2020. 2D Nitrogen−Doped Carbon Nanotubes/Graphene Hybrid as Bifunctional Oxygen Electrocatalyst for Long−Life Rechargeable Zn-Air Batteries. Adv. Funct. Mater. 30, 1906081.
Yan, B., Krishnamurthy, D., Hendon, C.H., Deshpande, S., Surendranath, Y., Viswanathan, V., 2017. Surface restructuring of nickel sulfide generates optimally coordinated active sites for oxygen reduction catalysis. Joule 1, 600-612.
Yan, X., Jia, Y., Odedairo, T., Zhao, X., Jin, Z., Zhu, Z., Yao, X., 2016. Activated carbon becomes active for oxygen reduction and hydrogen evolution reactions. Chem. Comm. 52, 8156-8159.
Yang, J., Xiang, F., Guo, H., Wang, L., Niu, X., 2020. Honeycomb-like porous carbon with N and S dual-doping as metal-free catalyst for the oxygen reduction reaction. Carbon 156, 514-522.
Yang, L., Jiang, S., Zhao, Y., Zhu, L., Chen, S., Wang, X., Wu, Q., Ma, J., Ma, Y., Hu, Z., 2011. Boron−doped carbon nanotubes as metal−free electrocatalysts for the oxygen

reduction reaction. Angew. Chem. Int. Ed. 50, 7132-7135.
Yang, L., Shui, J., Du, L., Shao, Y., Liu, J., Dai, L., Hu, Z., 2019. Carbon−based metal‐free ORR electrocatalysts for fuel cells: past, present, and future. Adv. Mater. 31, 1804799.
Yu, J., Chen, G., Sunarso, J., Zhu, Y., Ran, R., Zhu, Z., Zhou, W., Shao, Z., 2016a. Cobalt Oxide and Cobalt−Graphitic Carbon Core-Shell Based Catalysts with Remarkably High Oxygen Reduction Reaction Activity. Adv. Sci. 3, 1600060.
Yu, J., Ran, R., Zhong, Y., Zhou, W., Ni, M., Shao, Z., 2020a. Advances in porous perovskites: synthesis and electrocatalytic performance in fuel cells and metal–air batteries. Energy Environ. Mater. 3, 121-145.
Yu, J., Sunarso, J., Zhu, Y., Xu, X., Ran, R., Zhou, W., Shao, Z., 2016b. Activity and stability of Ruddlesden-Popper−type $La_{n+1}Ni_nO_{3n+1}$ (n= 1, 2, 3, and ∞) electrocatalysts for oxygen reduction and evolution reactions in alkaline media. Chem. Eur. J. 22, 2719-2727.
Yu, J., Sunarso, J., Zhuang, W., Yang, G., Zhong, Y., Zhou, W., Zhu, Z., Shao, Z., 2017. Synthesis of Highly Porous Metal−Free Oxygen Reduction Electrocatalysts in a Self−Sacrificial Bacterial Cellulose Microreactor. Adv. Sustainable Syst. 1, 1700045.
Yu, Y., Zhou, J., Sun, Z., 2020b. Novel 2D Transition−Metal Carbides: Ultrahigh Performance Electrocatalysts for Overall Water Splitting and Oxygen Reduction. Adv. Funct. Mater. 30, 2000570.
Zhang, S., Shang, N., Gao, S., Meng, T., Wang, T., Wang, Z., Gao, Y., Wang, C., 2021. Ultra dispersed Co supported on nitrogen-doped carbon: An efficient electrocatalyst for oxygen reduction reaction and Zn-air battery. Chem. Eng. Sci. 234, 116442.
Zhang, J., He, J., Hongying, Z., Li, R., Xinglong, G., 2020a. N, S dual-doped carbon nanosheet networks with hierarchical porosity derived from biomass of Allium cepa as efficient catalysts for oxygen reduction and Zn–air batteries. J. Mater. Sci. 55, 7464-7476.
Zhang, J., Xia, Z., Dai, L., 2015. Carbon-based electrocatalysts for advanced energy conversion and storage. Sci. Adv. 1, e1500564.
Zhao, H., Sun, C., Jin, Z., Wang, D.-W., Yan, X., Chen, Z., Zhu, G., Yao, X., 2015. Carbon for the oxygen reduction reaction: a defect mechanism. J. Mater. Chem. A 3, 11736-11739.

Graphical Abstract

Description

The novel N-doped graphitic carbon nanosheets with abundant topological defects and hierarchically porous structure were fabricated as an efficient metal-free electrocatalyst for oxygen reduction reaction in Zn-Air batteries.

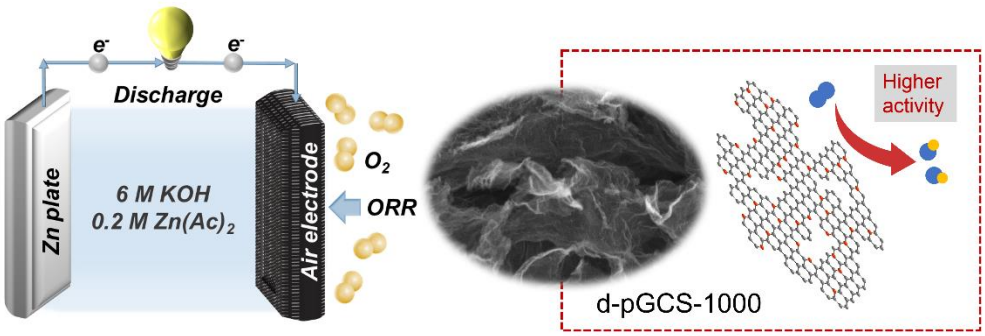
e-
e-
Discharge
Zn plate
6 M KOH
0.2 M Zn(Ac)2
Air electrode
O2
ORR
Higher activity
d-pGCS-1000